doi.org/10.36721/PJPS/2026.40.16377.1

Enhanced anti-inflammatory effects of (-)-linalool, (-)-borneol and β-caryophyllene via NF-κB/Nrf2 and arachidonic acid pathways

WanLin Wang[1,2], Kazi Sabnam Siddiqua[1], Yue Gao[1], Qiong Yi[1], Jiarong Yin[1] and Lu Wang[1]*

[1]The Engineering and Research Center for Southwest Bio-Pharmaceutical Resources of National Education Ministry of China, Guizhou University, Guiyang, China

[2]Department of Pharmacy, Sansui County People's Hospital, Sansui, China

Abstract: **Background**: Chronic immune-mediated inflammation remains difficult to treat with single-target approaches. Terpenoids are known to modulate immune responses, but whether specific combinations can produce enhanced effects and through which mechanisms is not well understood. **Objectives**: This study investigates whether a fixed-ratio combination (5:23:26) of (-)-Linalool, (-)-Borneol and β-Caryophyllene (Formula 1) exerts enhanced anti-inflammatory effects and explores the underlying molecular mechanisms. **Methods**: Two complementary models were used: release of slow-reacting substance of anaphylaxis (SRS-A) in isolated guinea pig ileum and LPS-activated RAW264.7 macrophages. PGE2, LTB4, NO and iNOS levels were measured. Network pharmacology, followed by experimental validation, identified key targets and pathways. Cellular morphology, apoptosis and NF-κB p65 nuclear accumulation were assessed by Hoechst 33342/PI staining and fluorescent plasmid transfection. **Results**: Formula 1 achieved 79.88% inhibition of SRS-A release, significantly surpassing every single component ($P < 0.001$) and the positive control quercetin. It also reduced PGE2, LTB4, NO and iNOS levels more effectively than any single compound. In LPS-stimulated macrophages, Formula 1 reduced cell deformation and apoptosis and markedly reduced p65 nuclear translocation. Mechanistically, it increased the Nrf2/HO-1 axis while down-regulating NF-κB and the arachidonic acid pathway. Notably, even when (-)-Linalool was reduced to one-tenth of its dose, Formula 1 maintained comparable efficacy. **Conclusions**: The combination of (-)-Linalool, (-)-Borneol and β-Caryophyllene produces enhanced anti-inflammatory effects through coordinated regulation of multiple pathways, as supported by the Highest Single Agent (HSA) model. These findings provide a basis for developing multi-target therapies for immune-mediated inflammatory diseases.

Keywords: Arachidonic acid; Inflammation; NF-κB; Terpenes; Pharmacological synergy

Submitted 02-03-2026 – Revised 21-05-2026 – Accepted 04-06-2026

INTRODUCTION

Chronic inflammatory diseases driven by dysregulated immune responses represent a formidable clinical challenge. Pathologies observed in global outbreaks such as COVID-19 (Qidwai, 2024), influenza (Chen *et al.*, 2025), Chikungunya (Kumar *et al.*, 2025) and Nipah virus (Cong *et al.*, 2025) underscore the manner in which excessive inflammatory cascades drive tissue damage. At the center of this complexity lies the nuclear factor-kappa B (NF-κB) pathway, which functions as a master regulator by coordinating the production of key pro-inflammatory cytokines, among them IL-1β, TNF-α and iNOS, along with central players in the arachidonic acid (AA) cascade (Capece *et al.*, 2022). Persistent NF-κB signaling remains a definitive hallmark of chronic inflammation. Parallel to this, the AA metabolic pathway via the action of cyclooxygenase-2 (COX-2) and 5-lipoxygenase (5-LOX) generates potent inflammatory eicosanoids, notably leukotriene B4 (LTB4) and prostaglandin E2 (PGE2), that sustain inflammatory damage (Taniguchi and Karin, 2018). Within this axis, 5-LOX activating protein (FLAP) serves as a critical facilitator for leukotriene biosynthesis (D Orazio and Mattoscio, 2024). Counterbalancing these pro-inflammatory forces, the nuclear factor erythroid 2-related factor 2 (Nrf2) orchestrates a critical cytoprotective response by upregulating antioxidant genes, among them heme oxygenase-1 (HO-1), thereby mitigating oxidative stress and suppressing inflammatory signaling (Zeng *et al.*, 2025). Given the intricate crosstalk between the NF-κB, AA and Nrf2 signaling nodes, a coordinated multi-pathway modulation likely offers a superior therapeutic threshold when compared to conventional single-target approaches (Niu *et al.*, 2024). Supporting this concept, recent investigations have shown that natural products can simultaneously regulate multiple inflammatory pathways. For example, artesunate promotes antitumor immunity by reprogramming macrophages via the STAT1/IRF1 axis (Hu *et al.*, 2025), while coniferyl aldehyde alleviates osteoarthritis by modulating glycolysis and histone lactylation (Pan *et al.*, 2026) and isoorientin suppresses macrophage pyroptosis through the KDM4A/NLRP3 pathway (Wang *et al.*, 2025). These findings illustrate the broad potential of plant-derived compounds in reshaping inflammatory networks.

**Corresponding author:* e-mail: wanglu7007@163.com

Article in Press

Terpenoids have garnered attention for their distinct immunomodulatory profiles. (-)-Linalool, (-)-Borneol and β-Caryophyllene are often key active components in various traditional anti-inflammatory medicinal plants. These compounds frequently coexist within the same plant. *Blumea balsamifera (L.) DC* is a representative example (Yaling *et al.*, 2021). Existing research indicates that (-)-Linalool exerts anti-inflammatory effects by regulating the TLR4/NF-κB signaling pathway (Riaz *et al.*, 2025). (-)-Borneol is the primary contributor to the anti-inflammatory activity in plant essential oils. It is capable of inhibiting the NF-κB pathway and AA metabolism (Xiao *et al.*, 2025). β-Caryophyllene, as an agonist of the cannabinoid CB2 receptor, can also inhibit the NF-κB pathway and alleviate inflammatory damage (Wang *et al.*, 2025). In line with these findings, new anti-inflammatory agents continue to be identified from natural sources. For instance, benzyl alcohol derivatives isolated from *Moringa oleifera* seeds displayed moderate inhibitory activity against NO production in macrophages, as confirmed by molecular docking (Wang *et al.*, 2024). Likewise, polysaccharides from *Ginkgo biloba* were shown to reduce the release of TNF-α, IL-6 and IL-1β by blocking the NF-κB signaling cascade (Zhang *et al.*, 2024). However, these findings are largely limited to individual compounds. A critical gap remains regarding the integrated immunopharmacology of defined multi-terpenoid combinations. Whether these chemical entities interact synergistically to recalibrate immune homeostasis remains unknown. Consequently, this study investigates the synergistic potential of a specific combination involving (-)-Linalool, (-)-Borneol and β-Caryophyllene. By integrating network pharmacology with an *in-vitro* macrophage model and an *ex-vivo* sensitized guinea pig ileum assay, this study was aimed at defining the molecular signature of this consortium and providing a rational basis for novel multi- target immunomodulatory strategies.

MATERIALS AND METHODS

Reagents

The compounds in the present study, including (-)-Linalool (CAS NO: 126-91-0, purity ≥ 98%), (-)-Borneol (CAS NO: 464-45-9, purity ≥ 98%), β-Caryophyllene (CAS NO: 87-44-5, purity ≥ 98%) and LPS (serotype O111:B4), were commercially sourced from Sigma-Aldrich (St. Louis, MO, USA). Figure S1 displays their molecular structures. Ovalbumin (OVA) was acquired from Solabio Company (Beijing, China). Quercetin was obtained from the China Food and Drug Administration. For cell viability and nuclear protein analysis, the nuclear protein extraction kit and MTS assay kit were sourced from Beyotime Biotechnology (Beijing, China). For protein quantification and RNA isolation, the BCA protein assay kit and RNA extraction kit were obtained from CoWin Biotechnology (Beijing, China). Fetal bovine serum (FBS) and Dulbecco's modified Eagle's medium (DMEM), essential for cell culture, were acquired from Gibco (Fort Worth, TX, USA). Primary antibodies for p-p65, p-IKKα/β, IKKα and RIPA lysis buffer were supplied by Cell Signaling Technologies (Danvers, USA). The following antibodies were supplied by ImmunoWay (Beijing, China): primary antibodies against P65, COX-2, 5-LOX, p-IκB-α, IκB-α, HO-1, Nrf2, β-actin and histone H3, as well as secondary antibodies against rabbit and mouse IgG. All drug treatments were prepared at the same total mass concentration to ensure equal drug exposure across groups. For *ex-vivo* experiments, each compound or Formula 1 was dissolved in DMSO, mixed with Tween-80 (1:1, v/v) and diluted with water to 1 mg/mL (final DMSO ≤ 0.1%, Tween-80 ≤ 0.5%); vehicle controls contained the same solvents. For *in-vitro* assays, stock solutions in DMSO were prepared as follows: (-)-Borneol and β-Caryophyllene at 50 mg/mL each, (-)-Linalool and Formula 1 (5:23:26 mass ratio) at 100 mg/mL, stored at −4 °C. Before use, they were diluted with culture medium to 80 μg/mL (final DMSO ≤ 0.1%) and a 0.1% DMSO solvent control was included.

SRS-A assay

Male guinea pigs (180 ± 10 g) were obtained from the Chongqing Tengxin Experimental Animal Centre (Animal License No. SYXK (Yu) 2022-0006). All animals were acclimatized in a clean-grade facility at Guizhou University in an environment with temperature controlled at 20-25°C, a 12-hour light/dark cycle and relative humidity (55 ± 5%). Standard water and chow were supplied ad libitum. All animal procedures received approval from the Animal Experiment Ethics Committee of Guizhou University (Approval Number: EAE–GZU–2021–E026). Formula 1 was prepared at the ((-)-Linalool: (-)-Borneol: β-Caryophyllene) 5:23:26 mass ratio, exactly matching the GC-MS profile of *Blumea balsamifera (L.) DC* (Xueyan *et al.*, 2019). Animals were deeply anaesthetised by ether inhalation and then euthanised by cervical dislocation before tissue collection. To assess whether this natural ratio is pharmacologically optimized, Formula 2 (equal ratio, 1:1:1) and Formula 3 (random ratio, 1:2:7) were also tested. The slow-reacting substance of anaphylaxis (SRS-A) bioassay was performed according to an established method (Xianfang *et al.*, 2024). In short, an *ex-vivo* anaphylaxis model was established using OVA-sensitized guinea pigs. The ileum was isolated and mounted in an organ bath and the contractile response induced by exogenous histamine was quantified for calibration. After the ileum contraction stabilized, SRS-A and the test compounds were introduced. The experimental groups were assigned as follows: A control group (SRS-A alone), experimental groups (SRS-A plus one test formulation), a positive control group (SRS-A plus quercetin) and vehicle control groups (SRS-A plus 0.1% DMSO or 0.5% Tween-80). Each condition was tested in triplicate.. Contraction curves of the guinea pig ileum were recorded and the

Article in Press

average contraction amplitude for each group was calculated. To determine SRS-A content, contractile tension was compared against standard curves generated with known concentrations of histamine and SRS-A. The inhibition rate for each group was then calculated by comparing the contractile amplitude of the experimental group with that of the control group, using the following formula: Inhibition rate (%) = [(Control group − Experimental group) / Control group] × 100, with "Control" and "Experimental" referring to the contraction amplitudes in the control and experimental groups, respectively.

Cell culture, reagents and experimental groups

RAW264.7 macrophages were sourced from the Kunming Cell Collection, CAS (Kunming, China). MCF-7 cells were sourced from the CAS (Beijing bena culture collection). In a humidified 5% CO_2 atmosphere at 37 °C, DMEM enriched with 1% penicillin/streptomycin and 10% FBS served as the culture medium for cell propagation. RAW264.7 macrophages were detached using a cell scraper in ice-cold PBS without trypsin-EDTA. MCF-7 cells were detached with 0.25% (w/v) trypsin-EDTA for 2 min at 37 °C. The harvested cells were then subjected to three washes with PBS (0.1 M, pH 7.0) for use in subsequent experiments. The pEGFP-N1-P65 fluorescent plasmid was constructed previously in prior work, while the empty pEGFP-N1 plasmid vector was supplied by MiaoLing Biotechnology Co., Ltd. (Wuhan, China). For *in-vitro* assays, RAW 264.7 cells were seeded, pre-cultured for 6 h and then divided into the following six treatment groups: (1) blank control group (Con), (2) model group (LPS), (3) three drug-treated groups (40, 60 and 80 μg/mL) and (4) a drug control group (80 μg/mL alone). After 12 h of treatment, cells and culture supernatants were collected for subsequent analysis. Three replicate wells were prepared for each experimental condition. Treatment durations were optimized by preliminary time-course experiments. A 12 h treatment was used for qPCR, Western blot, ELISA, Griess assay and Hoechst/PI staining; a 24 h treatment was used for MTS cell viability assay. For NF-κB p65 nuclear translocation, cells were transfected for 12 h and then treated for another 12 h.

Cell viability assay

Following established protocols, the MTS assay was employed to simultaneously evaluate the viability of RAW264.7 macrophages and the potential cytotoxic effects of the test compounds. For this purpose, the cells were first plated into 96-well microplates at a density of 1 × 10^5 cells per well and then cultured overnight to allow attachment. The next day, the culture medium was exchanged for fresh medium containing a range of concentrations (0, 40, 60, 80, 120, 250 and 500 μg/mL) of the compounds under investigation. Following a 24 h incubation period, cell proliferation and viability were determined by adding 20 μL of MTS reagent to each well. The plates were then placed back into the incubator for an additional 4 h at 37 °C to facilitate the bioreduction of MTS into soluble formazan crystals. Finally, the formazan quantity, directly proportional to viable cell number, was measured by recording the absorbance at 490 nm using a microplate reader (Thermo Fisher Scientific, USA). To assess the impact of the Formula 1 under inflammatory conditions, the Formula 1 treatment group was also evaluated under co-treatment with LPS.

Hochest33342 and PI double staining

Cell apoptosis and necrosis were assessed using a commercial Apoptosis and Necrosis Assay Kit. RAW264.7 cells were plated at a density of 4 × 10^5 cells per well into 12-well plates and subjected to the respective treatments. After incubation, cells were rinsed twice with PBS. Subsequently, the cell nuclei were then stained by incubation with Hoechst 33342 (5 μg/mL), which labels all nuclei and propidium iodide (PI, 2 μg/mL), selectively staining nuclei of cells undergoing secondary necrosis or late-stage apoptosis, following a 15 min incubation at 4°C in the dark. After staining, cells were promptly visualized and imaged with an inverted fluorescence microscope (OLYMPUS IX71, Tokyo, Japan).

ELISA and griess assay

Following the experimental design, RAW264.7 cells were seeded into 24-well plates at 2 × 10^5 cells/well and pre-cultured for 6 h to facilitate adhesion. Subsequently, the cells were incubated for 12 h with the test compounds in media supplemented with or without LPS (500 ng/mL). After incubation, the cell-free supernatant was harvested from each group and centrifuged to remove cellular debris. PGE2 and LTB4 levels in the supernatant were measured by specific commercial ELISA kits (GeneMei Co., Ltd., Wuhan, China). The concentration of nitric oxide (NO) was determined using a Griess reagent kit (Nanjing Bioengineering Co., Ltd., Nanjing, China), in line with the manufacturer's guidelines.

qPCR and Western blotting

To examine the expression of target genes and their corresponding proteins, qPCR and Western blotting were carried out as per previously reported protocols (Liao *et al.*, 2021). For transcriptional evaluation, RAW264.7 cells were first plated into 6-well plates to achieve a density of 6 × 10^5 cells per well. Following a 6 h period to allow for cell attachment, the cultures were exposed to the test compounds, either alone or in combination with LPS (500 ng/mL), for an additional 12 h. Total RNA was subsequently isolated using a commercially available RNA extraction kit, strictly following the supplier's operating instructions. The cDNA was generated using the Quant Reverse Transcriptase Kit (Tiangen, Beijing, China). The qPCR reactions were performed on a real-time PCR system with a SYBR Green RT-PCR kit (Thermo Fisher Scientific, USA). Gene-specific primers were designed using Primer Premier 5.0 software,

Article in Press

employing mouse mRNA sequences available in the NCBI database (sequences provided in Table S1). Relative quantification of gene expression was achieved by the comparative Ct (2-ΔΔCt) method, with GAPDH serving as the endogenous control to normalize the data. For protein expression analysis, cells were cultured and treated under identical conditions as described for the qPCR experiments. The protein concentration in the lysate was analysed using the BCA protein assay. Total cellular proteins were extracted by RIPA lysis buffer that was freshly prepared with both protease and phosphatase inhibitor cocktails. To obtain subcellular fractions, nuclear and cytoplasmic proteins were separated using a commercial nuclear protein extraction kit. For immunoblotting, 20 μg of protein sample was loaded into each lane and resolved by 10% SDS-PAGE, followed by electrotransfer to a PVDF membrane (Bio-Rad Laboratories, USA). Following transfer, incubate the membrane in TBST supplemented with 5% (w/v) skim milk at ambient temperature for 1 h to reduce non-specific binding. The membranes were then kept overnight at 4°C with specific primary antibodies directed against p-p65 (1:1000), p-IKKα/β (1:1000), IKKα (1:1000), HO-1 (1:500), COX-2 (1:1000), p65 (1:1000), IκB-α (1:1000), p-IκB-α (1:1000), 5-LOX (1:1000), Nrf2 (1:1000), β-actin (1:1500) and histone H3 (1:500). Following extensive washing with TBST, the membranes were exposed to appropriate HRP-conjugated secondary antibodies (1:50,000) at ambient temperature for 1 h. Visualization of immunoreactive bands was performed using an ECL kit (Bio-Rad, USA) and images were captured with a UVP ChemStudio/Touch system (Analytik Jena, Germany). The resulting band intensities were quantified densitometrically using ImageJ software (National Institutes of Health, USA). To ensure accurate comparison, the expression levels of target proteins were standardized to β-actin for total and cytoplasmic proteins and to histone H3 for nuclear proteins.

Analysis of NF-κB P65 nuclear localization

RAW264.7 macrophages were unsuitable for fluorescence imaging of p65 nuclear translocation due to low transfection efficiency and poor adherence during processing. Therefore, MCF-7 cells, which are widely used for imaging assays because of their stable adherence and high transfection efficiency, were employed to visualize the effect of Formula 1 on p65 localization. The NF-κB pathway is highly conserved and the functional consequences of NF-κB inhibition were further validated in RAW264.7 macrophages by measuring downstream inflammatory mediators. To visualize the subcellular localization of NF-κB P65, MCF-7 cells were seeded in 24-well plates and cultured for 24 h to allow attachment. Cells were then introduced with the pEGFP-N1-P65 plasmid via Lipofectamine™ 3000 reagent (Invitrogen, USA), as per the producer's instructions, using a ratio of 1.5 μL transfection reagent per 1 μg of plasmid. After 12 h of transfection, cells were assigned to the following treatment groups and incubated for an additional 12 h: (1) control group (Con); (2) model group (stimulated with LPS); and (3) drug-treated group (co-treated with LPS and Formula 1). The redistribution of EGFP-tagged P65 protein to the nucleus was subsequently observed and imaged using fluorescence microscopy.

Network pharmacological analysis

Underlying mechanisms were explored by identifying common targets of the active compounds ((-)-Linalool, (-)-Borneol and β-Caryophyllene) and inflammation-related pathways. Compound structures and targets were performed using TCMSP (accessible at https://www.tcmsp-e.com) (Liu *et al.*, 2026). Inflammation-associated targets were obtained from the OMIM (accessible at https://omim.org) and GeneCards (accessible at https://www.genecards.org) (Pan *et al.*, 2026). Potential therapeutic targets were analyzed via a PPI network constructed using STRING and visualized with Cytoscape 3.10.3 (Luo *et al.*, 2025). Enrichment assessment for KEGG pathways and GO terms was performed with the aid of Metascape (Cui *et al.*, 2026) (https://metascape.org). The online platform was used to visualize the results (accessible at http://www.bioinformatics.com). Molecular docking of the compounds (structures sourced from PubChem) with key targets was conducted using CB-Dock 2 (Jiang *et al.*, 2026) (https://cadd.labshare.cn/cb-dock2/). Binding affinities were evaluated by Vina scores, with values < –5 kcal/mol considered indicative of stable binding (Karaoli *et al.*, 2026).

Statistical analysis

All analyses were performed with three biological replicates (n = 3) in accordance with the 3R principle to minimize animal use. Data are presented as mean ± SD. Normality and homogeneity of variance were assessed by the Shapiro-Wilk and Levene's tests, respectively. One-way ANOVA was used to compare nine groups, followed by Tukey's HSD post hoc test at a significance level of $P < 0.05$. Effect sizes (η^2, ω^2, Cohen's d) were calculated and Dunnett's correction was applied for comparisons versus the control. $P < 0.05$ was considered significant. SPSS v27 was used. Because each terpenoid in Formula 1 was at a much lower individual dose than in its single-agent test and SRS-A was a single-concentration assay, classical CI/Bliss analysis was not feasible. Instead, synergy was assessed using the Highest Single Agent (HSA) model (Huang *et al.*, 2022; Vlot *et al.*, 2019).

RESULTS

Inhibitory effects of compounds on SRS-A release in a guinea pig model

Using the classical guinea pig ileum assay (with no solvent effect from 0.1% DMSO or 0.5% Tween-80), combinations of (-)-Borneol, (-)-Linalool and β-Caryophyllene were tested for SRS-A inhibition (Table 1, Fig. S2).

Article in Press

Table 1: Effects of compounds on pulmonary SRS-A production and ileal contractile tone in guinea pigs.

Group	Contractile tone (g)	SRS-A production (U/g tissue)	Inhibition rate (%)	letter
Formula 1	0.064 ± 0.01	35.62 ± 2.11	79.875 ± 0.35	a
Quercetin	0.119 ± 0.01	52.25 ± 2.51	70.481 ± 1.41	b
(-)-Linalool	0.151 ± 0.01	74.67 ± 6.12	57.810 ± 3.45	c
Formula 2	0.169 ± 0.02	85.36 ± 9.81	51.775 ± 5.54	c
Formula 3	0.175 ± 0.01	88.27 ± 4.37	50.129 ± 2.47	c
β-Caryophyllene	0.241 ± 0.02	111.74 ± 8.81	36.870 ± 4.97	d
(-)-Borneol	0.286 ± 0.01	157.73 ± 1.61	10.884 ± 0.90	e
Solvent	0.317 ± 0.01	174.55 ± 2.98	1.383 ± 1.68	f
Control	0.318 ± 0.01	177.16 ± 6.20	-	f

SRS-A only as a control group; 0.1% DMSO and 0.5% Tween-80 as a solvent group. 0.1% compounds as an experimental group; Quercetin as a positive control for medicine. Data are presented as mean ± SD (n = 3). One-way ANOVA followed by Tukey's HSD post hoc test. Groups with different superscript letters (a-f) are significantly different ($P < 0.05$). Groups sharing the same letter are not significantly different.

One-way ANOVA revealed significant intergroup differences [$F(8,18) = 255.42$, $P < 0.001$, $\eta^2 = 0.991$, $\omega^2 = 0.987$]. The low standard deviation (SD = 0.353%) and large effect size support the reliability of n = 3. Tukey's HSD post hoc test confirmed no difference between solvent and blank controls ($P = 0.9996$). All treatments lowered SRS-A compared to control ($P < 0.05$). Formula 1 showed the strongest activity (79.88% inhibition), achieved with each terpenoid at only one-tenth to one-third of the single-agent dose, surpassing each monomer ($P < 0.001$) and quercetin ($P = 0.043$) was selected for further study. (-)-Linalool, Formula 2 and Formula 3 had moderate, comparable efficacy ($P > 0.05$), while β-Caryophyllene and (-)-Borneol had weaker but significant effects. According to the HSA model, this indicates an enhanced anti-inflammatory effect (Fig. S3). Superscript letters (a-f) in table 1 denote Tukey HSD homogeneous subsets; full pairwise comparisons are provided in table S2. A dose-reduction experiment further showed that even at one-tenth of the (-)-Linalool dose, Formula 1 retained comparable efficacy.

Effect of compounds on RAW264.7 cell viability

In order to assess the potential cytotoxicity of the test compounds, the viability of RAW264.7 cells was evaluated using the MTS assay after 24 h of exposure. As illustrated in figure 1, 0.1% DMSO had no significant effect on cell viability, confirming the absence of confounding solvent effects. Neither the individual compounds ((-)-Linalool, (-)-Borneol and β-Caryophyllene) nor their combination (Formula 1) exhibited significant cytotoxicity at concentrations up to 500 μg/mL. Based on these results, for all subsequent experiments, non-cytotoxic concentrations within the range of 0 to 80 μg/mL were selected for treatment.

Effect of compounds on LPS-induced production of inflammatory mediators

The levels of key inflammatory mediators such as LTB4, PGE2, NO and iNOS in the cell culture supernatant were determined using ELISA and Griess reagent. As illustrated in figure 2, LPS stimulation notably upregulated the release of LTB4 (A), PGE2 (B), NO (C) and iNOS (D). At the selected non-cytotoxic concentrations, the combination of (-)-Linalool, (-)-Borneol and β-Caryophyllene (Formula 1) significantly suppressed the production of all these mediators. In contrast, among the individual compounds, only (-)-Linalool exhibited significant inhibitory effects on specific mediators. Notably, Formula 1 achieved comparable anti-inflammatory efficacy with a substantially reduced amount of (-)-Linalool, suggesting a synergistic interaction among the constituents.

Impact of Formula 1 on the morphology and apoptosis of LPS-induced RAW264.7 cells

The cells were exposed to varying concentrations of Formula 1 (0–500 μg/mL) while being stimulated with LPS (500 ng/mL) for a period of 24 h. Cytotoxicity was evaluated using the MTS assay (Fig. 3), which revealed no significant loss of cell viability following Formula 1 exposure versus the control group ($P > 0.05$; Fig. 3A). Furthermore, Formula 1 partially mitigated the LPS-induced morphological changes in RAW264.7 cells (Fig. 3C). Hoechst 33342/PI double staining further demonstrated that LPS stimulation led to a significant increase in the percentage of PI-positive (necrotic/late apoptotic) cells relative to total cells (Hoechst-stained), compared with the control (Fig. 3B). However, Formula 1 treatment dose-dependently reduced this ratio (Fig. 3D). Collectively, these results demonstrate that Formula 1 at concentrations of 40–80 μg/mL significantly inhibits LPS-induced cell death in RAW264.7 macrophages, further supporting its anti-inflammatory activity at doses below 80 μg/mL.

Effects of Formula 1 on IL-1β and TNF-α expression

Recognized as key pro-inflammatory cytokines, IL-1β and TNF-α play indispensable roles in recruiting immune cells to inflammatory sites. To further investigate the potential anti-inflammatory effects of Formula 1, their expression levels were assessed at both the protein and transcriptional levels.

Article in Press

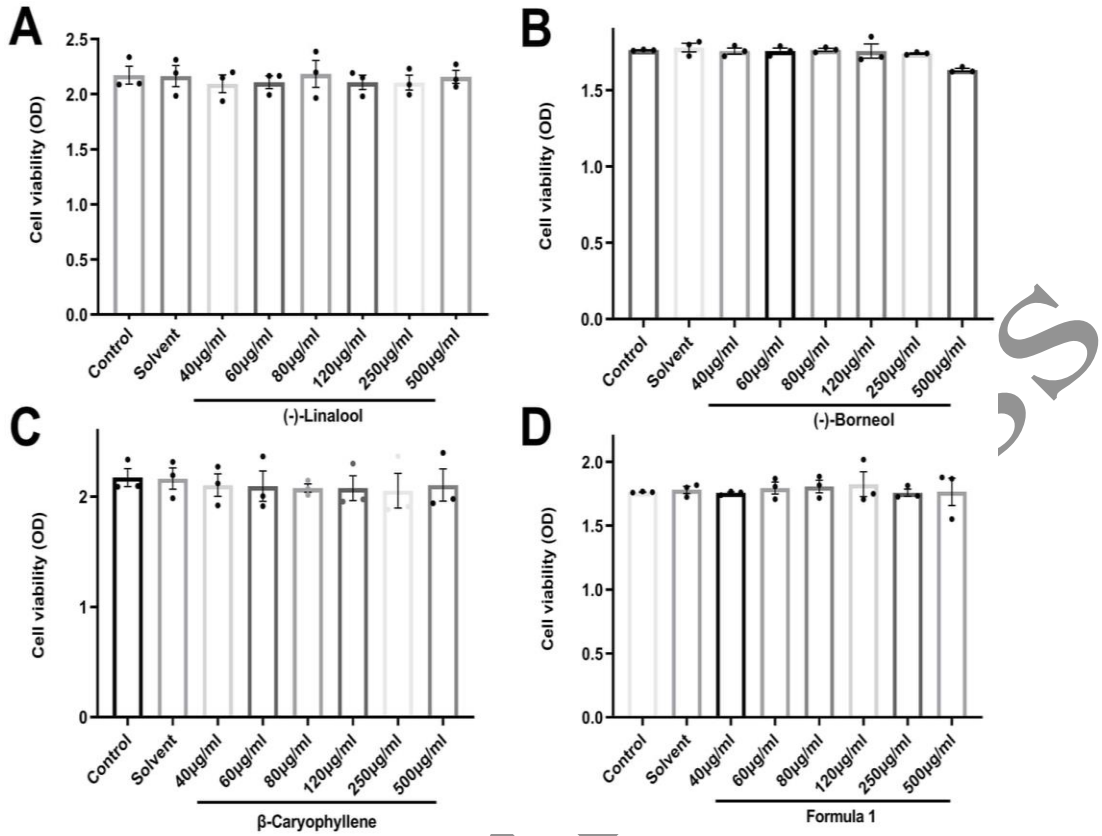


Fig. 1: Effects of (-)-Linalool (A); (-)-Borneol (B); β-Caryophyllene (C); and Formula 1; (D) on the viability of RAW264.7 cells, as determined by the MTS assay. Data are presented as the mean ± SD (n = 3).

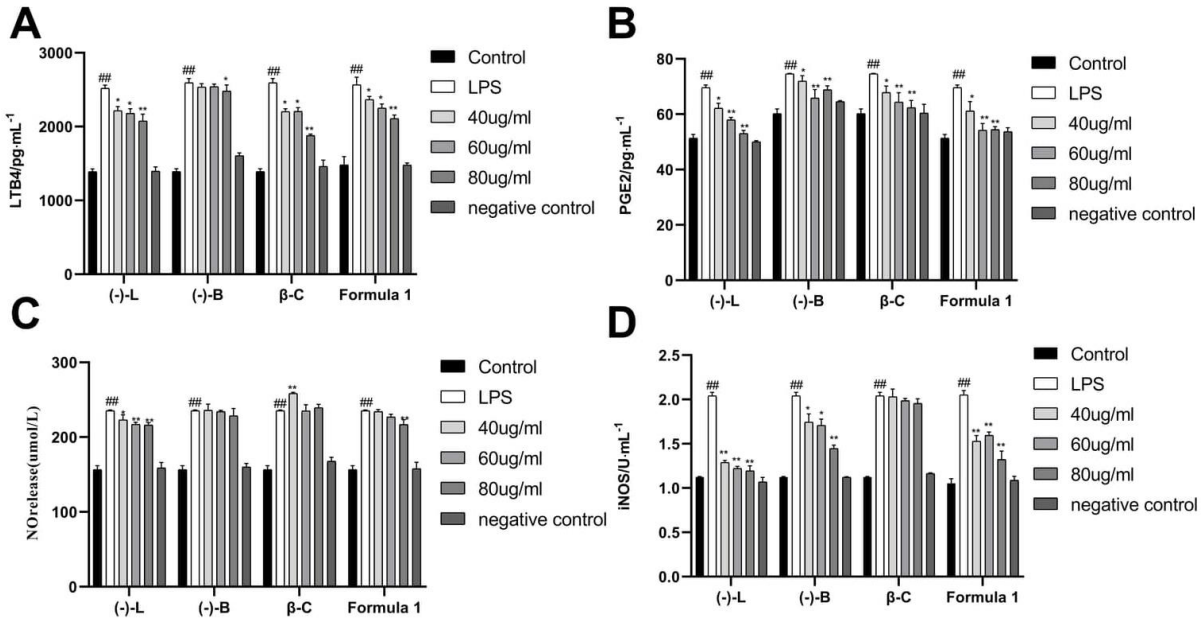


Fig. 2: Effects of compounds on the LPS-induced production of inflammatory mediators in RAW 264.7 cells. Levels of (A) LTB4; (B) PGE2 (by ELISA); (C) NO and; (D) iNOS (by Griess assay) in cell culture supernatants were measured after treatment with various drug concentrations (0-80 μg/mL). Data are expressed as the mean ± SD of three independent experiments (n = 3). #P < 0.05, ##P < 0.01 vs. control group; *P < 0.05, **P < 0.01 vs. LPS group. Abbreviations: (-)-L, (-)-Linalool; (-)-B, (-)-Borneol; β-C, β-Caryophyllene; Formula 1, fixed-ratio combination (5:23:26).

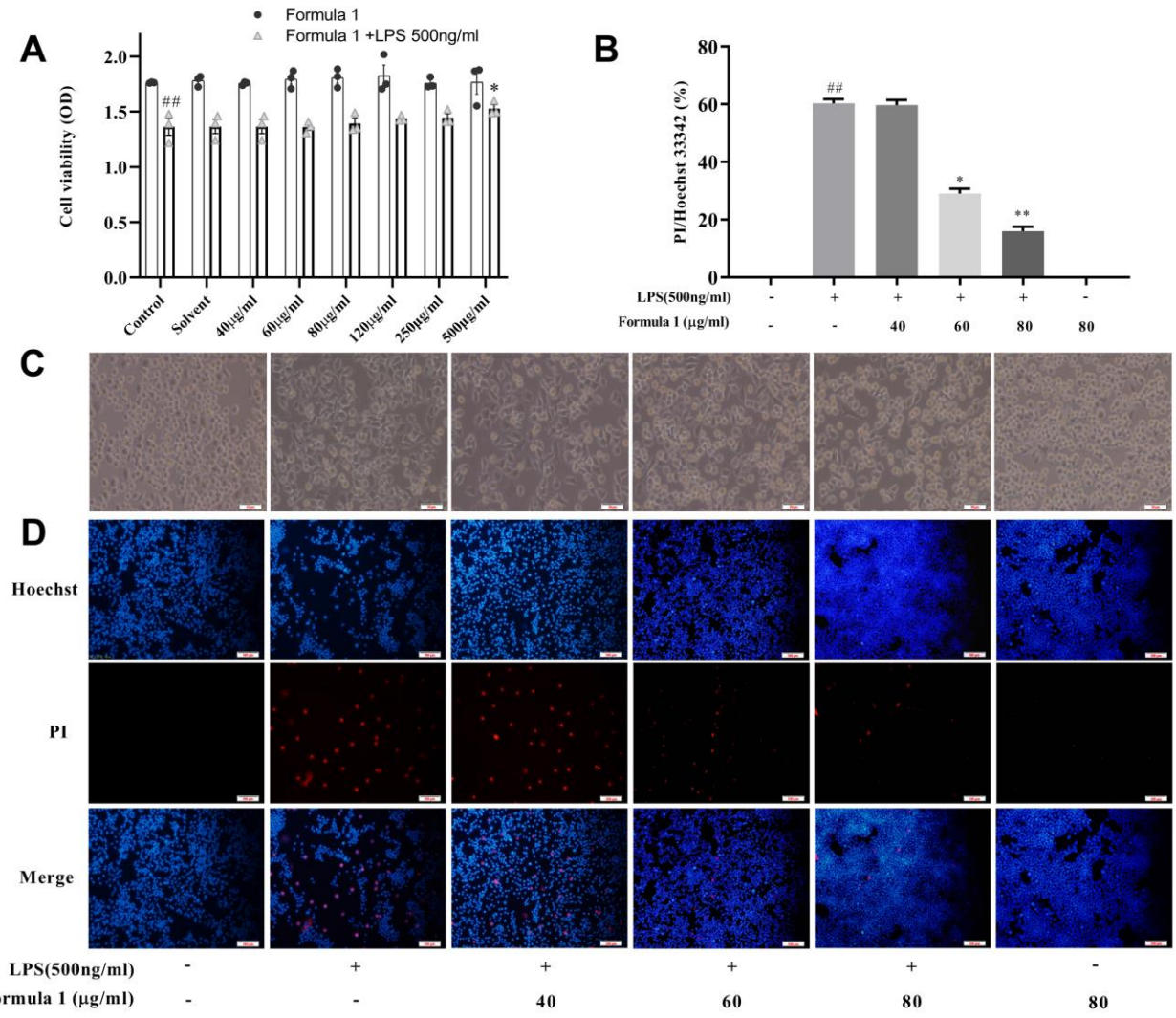


Fig. 3: Effect of Formula 1 on the morphology and apoptosis of LPS-induced RAW264.7 cells. (A) Cell viability was measured by MTS assay after treatment with Formula 1 (0-500 μg/mL) for 24 h; (B) Quantitative analysis of the ratio of PI-positive (necrotic/apoptotic) cells to total cells (Hoechst 33342-positive); (C) Morphological changes of cells observed under an inverted microscope, scale bar = 50 μm (20×); representative fields of view are shown for each group; (D) Fluorescence images of cells double-stained with Hoechst 33342 (blue, all nuclei) and PI (red, necrotic/late apoptotic cells), scale bar = 100 μm (10×). Data are presented as the mean ± SD (n = 3). #P < 0.05, ##P < 0.01 vs. control group; *P < 0.05, **P < 0.01 vs. LPS group. All images are representative of three independent experiments.

As illustrated in figure. 4, ELISA and qPCR analyses consistently demonstrated that Formula 1 significantly suppressed the LPS-induced production of IL-1β and TNF-α in a concentration-dependent fashion. Collectively, these findings provide further support for the potent anti-inflammatory efficacy of Formula 1.

Network pharmacological analysis of Formula 1 against inflammation

Network analysis identified 12 common targets shared by the active constituents of Formula 1 [(-)-Linalool, (-)-Borneol and β-Caryophyllene] and inflammation-related genes, suggesting their potential relevance as therapeutic targets (Fig. S4A).

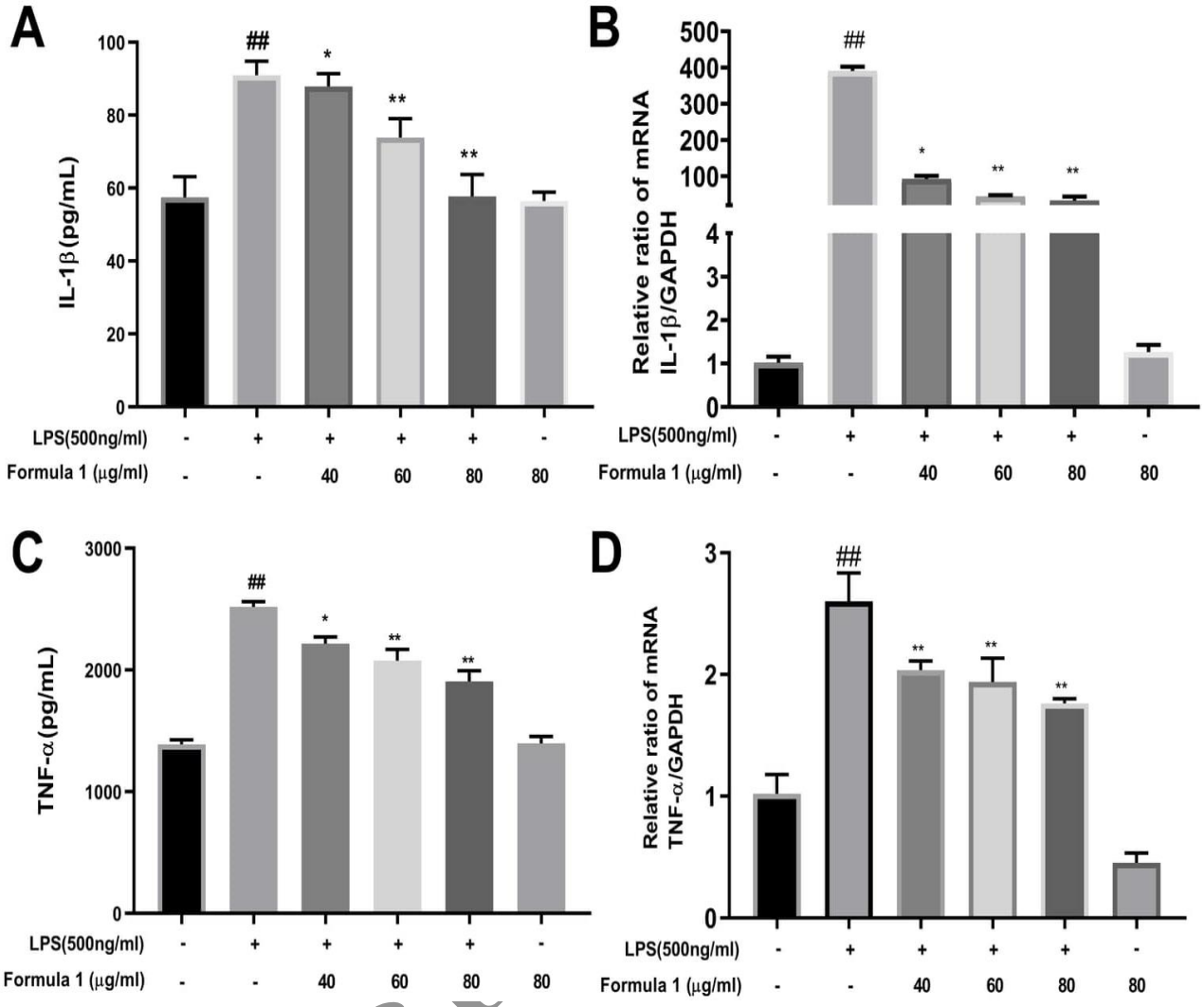


Fig. 4: Effects of Formula 1 on the expression of pro-inflammatory cytokines in LPS-induced RAW 264.7 cells. The mRNA (qPCR) and protein (ELISA) levels of IL-1β (A, B) and TNF-α; (C, D) were determined by qPCR and ELISA, respectively, after treatment with Formula 1 at concentrations ranging from 0 to 80 μg/mL. All data are presented as the mean ± SD (n = 3). #P < 0.05, ##P < 0.01 vs. control group; *P < 0.05, **P < 0.01 vs. LPS group.

A compound-target-pathway-disease network further illustrated these interactions (Fig. S4B). A PPI network derived from the common targets consisted of 10 nodes and 22 edges. Based on degree centrality, the top 6 hub targets were selected as the threshold for identifying key nodes. These key hub targets — including prostaglandin G/H synthase 2 (PTGS2/COX-2), retinoic acid receptor RXR-α (RXRA), vascular endothelial growth factor receptor 2 (KDR/VEGFR2), sodium-dependent dopamine transporter (SLC6A3), cytochrome P450-cam (CYP2C9) and interleukin-6 (IL-6) were identified based on high degree centrality (Fig. S4C). Enrichment analysis via GO and KEGG pathways conducted on these 12 targets revealed their association with critical inflammatory processes. According to GO analysis, enrichment was observed in biological processes and molecular functions associated with the prostaglandin-endoperoxide synthase activity, cyclooxygenase pathway, arachidonic acid (AA) metabolism, inflammatory response, oxidative stress and apoptosis (Fig. S4D). KEGG pathway analysis further linked these targets to key signaling pathways, including lipid and atherosclerosis, AA metabolism and the IL-17 signaling pathway (Fig. S4E). To validate potential interactions, molecular docking analyses were carried out for these three compounds against 12 core targets (Fig. S5). Multiple pairs exhibited significantly stable binding interactions (Vina score < −5 kcal/mol). The top five pairs by binding affinity included (-)-Linalool with KDR and β-Caryophyllene with SLC6A3, CYP2C9, RXRA and PTGS2, the molecular docking results are shown in figure 5. Based on these predictions and pathway enrichment analysis, the AA metabolism pathway and its key enzyme, PTGS2/COX-2, were experimentally validated, as this pathway was most relevant to acute inflammation. Other predicted targets were not experimentally tested due to low relevance or technical constraints.

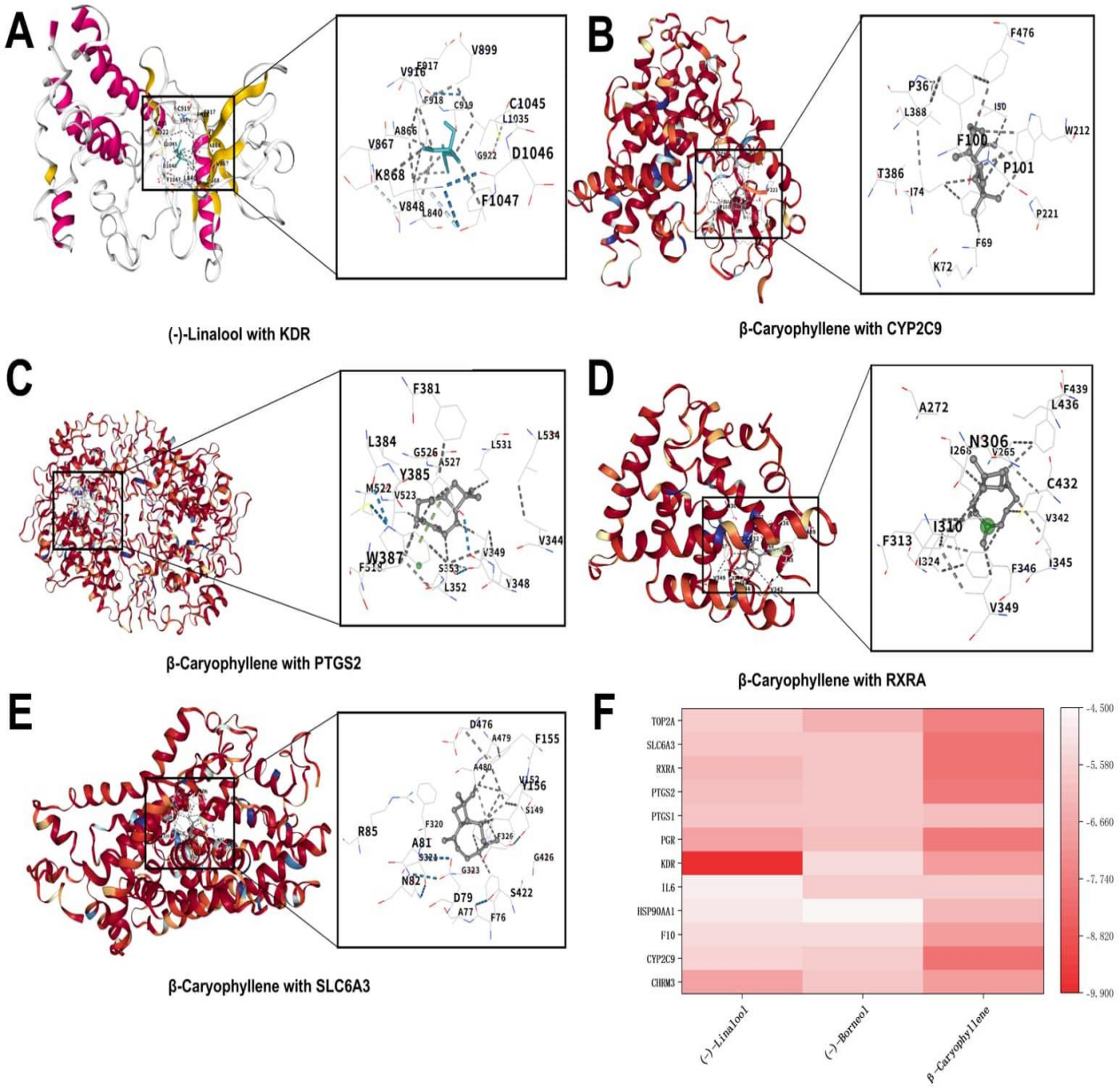


Fig. 5: Molecular docking diagrams showing the top five compounds by affinity score in combination with protein. (A) (-)-Linalool with KDR; (B) β-Caryophyllene with CYP2C9; (C) β-Caryophyllene with PFGS2; (D) β-Caryophyllene with RXRA; (E) β-Caryophyllene with SLC6A3. Detailed binding residues for the β-Caryophyllene with PTGS2 complex are described in the discussion; (F) Molecular docking heatmap showing binding affinities (Vina score, kcal/mol) between the three compounds and 12 core targets. Warmer colors (red) indicate stronger binding (more negative scores).

Formula 1 inhibits the activation of the AA signaling pathway

COX-2 (gene name: PTGS2), 5-LOX and FLAP are key enzymes in the AA metabolic pathway, which mediates the synthesis of pro-inflammatory mediators, including LTB4 and PGE2 (Choi *et al.*, 2010). Guided by network pharmacology predictions, the impact of Formula 1 on this pathway was experimentally evaluated. As shown in figure 6, LPS stimulation significantly upregulated the expression of proteins involved in the AA pathway. In contrast, treatment with Formula 1 markedly attenuated the LPS-induced elevation of COX-2, 5-LOX and FLAP expression.

Formula 1 inhibits the activation of the NF-κB signaling pathway

As predicted through network pharmacology analysis, RXR-α (Xu *et al.*, 2024) and PTGS2 (Cortez *et al.*, 2024) act as antagonists of NF-κB activity and are implicated in the suppression of inflammatory responses.

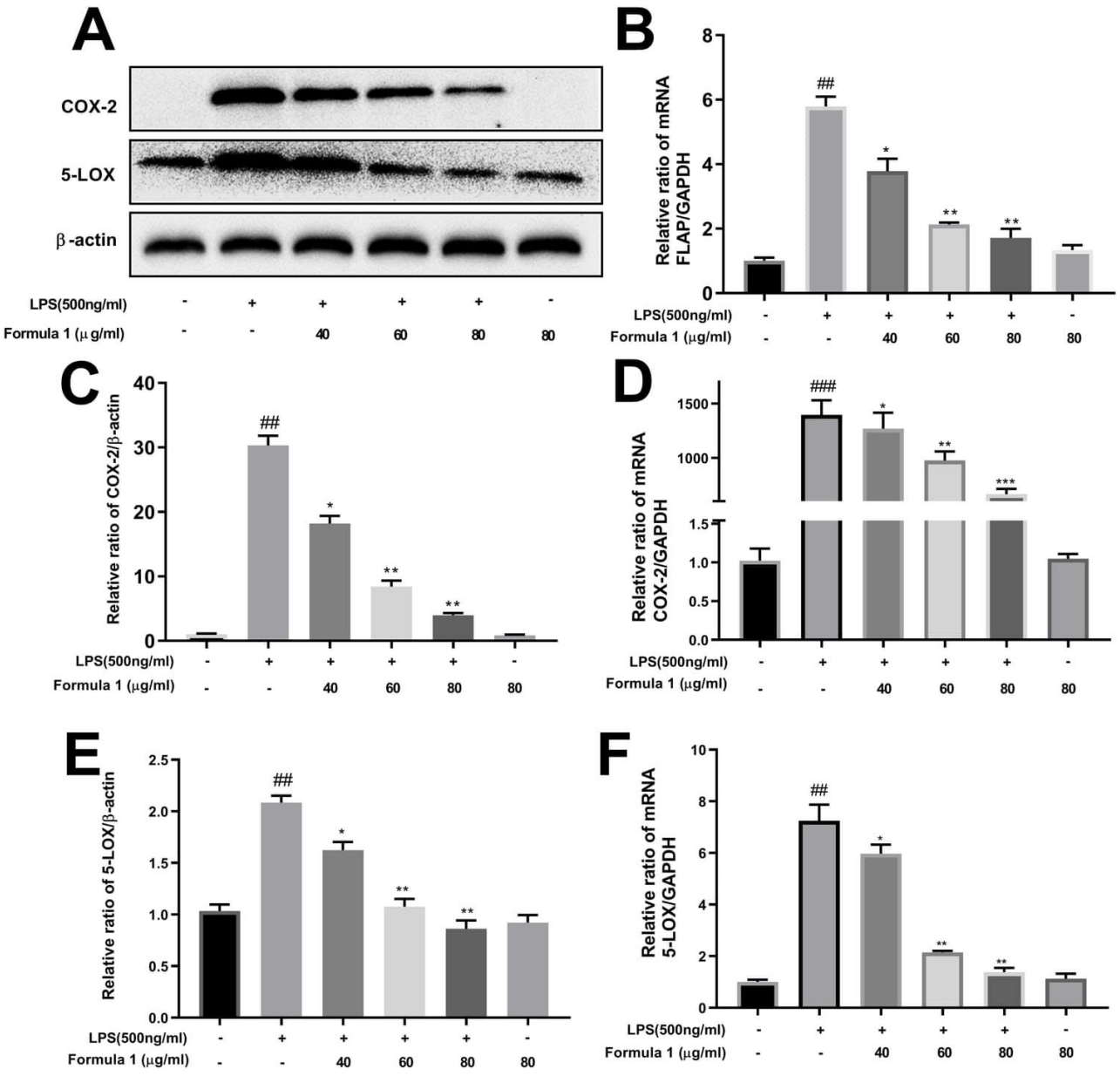


Fig. 6: Effects of Formula 1 on the AA signaling pathway in LPS-induced RAW264.7 cells. (A) Representative Western blot images of COX-2 and 5-LOX protein levels; (B) mRNA expression levels of FLAP; (C, D) Protein and mRNA expression levels of COX-2; (E, F) Protein and mRNA expression levels of 5-LOX. Data are presented as the mean ± SD from three independent experiments. #$P < 0.05$, ##$P < 0.01$, ###$P < 0.001$ vs. control group; *$P < 0.05$, **$P < 0.01$ vs. LPS group.

In contrast, VEGFR2 was identified as an activator of the pro-inflammatory NF-κB pathway (Wilkens *et al.*, 2024). These opposing regulatory roles prompted further experimental investigation of the NF-κB signaling pathway. As a master switch for inflammatory responses, the NF-κB signaling pathway is implicated in chronic immune regulation. Activation of the pathway can promote the expression of pro-inflammatory cytokines and suppress immunosuppressive responses, resulting in net inflammatory and apoptotic outcomes. As shown in figure 7, LPS stimulation markedly activated the NF-κB pathway, as evidenced by the upregulation of phosphorylation of IKKα/β, IκB-α and P65, along with decreased levels of IκB-α. Treatment with Formula 1 markedly reversed these changes, suppressing the LPS-induced upregulation of p-P65, p-IκB-α and p-IKKα/β and restoring IκB-α expression. Nuclear translocation of P65 is a signature feature of NF-κB pathway activation. Using live-cell imaging of an EGFP-tagged P65 construct, LPS stimulation was observed to promote P65 nuclear accumulation, which was effectively attenuated by co-treatment with 80 μg/mL Formula 1 (Fig. 8).

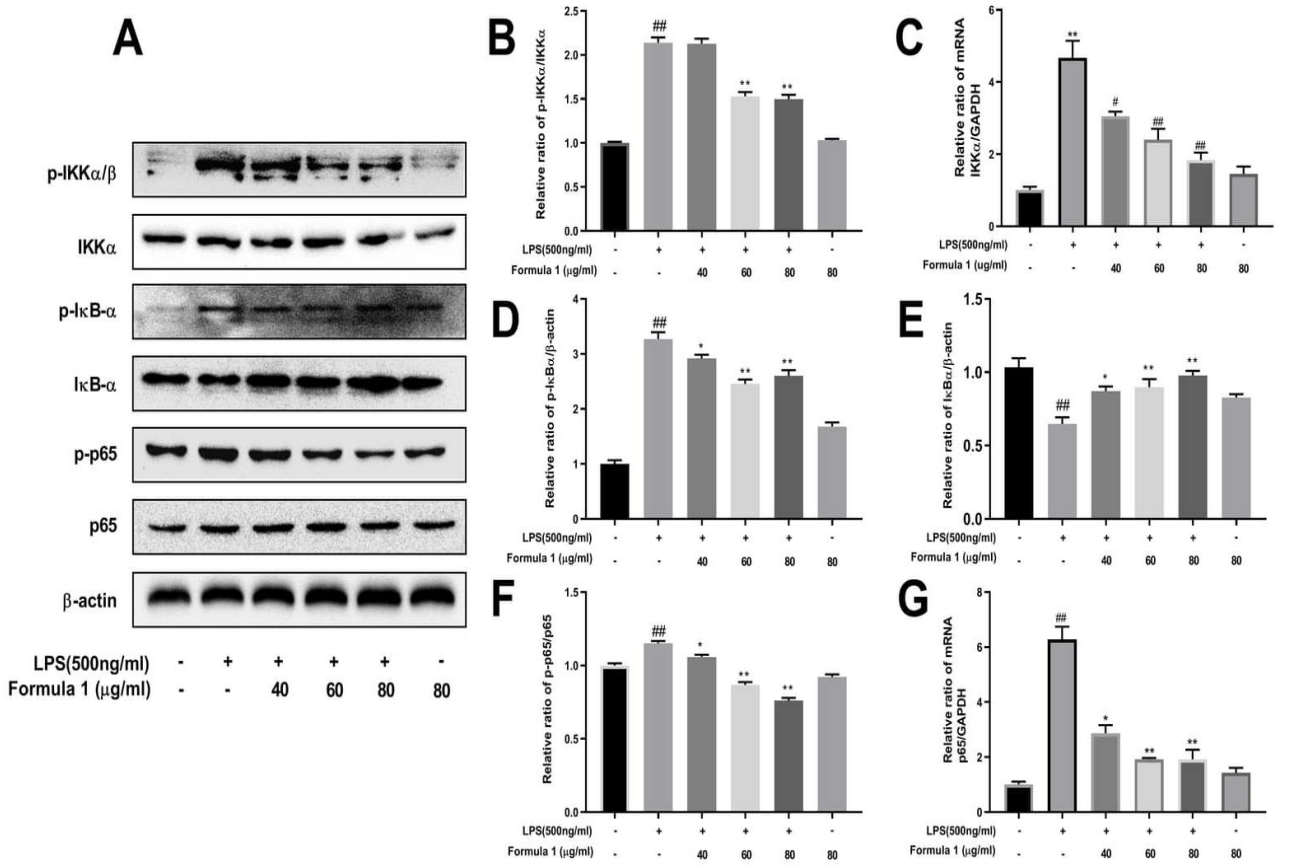


Fig. 7: Effects of Formula 1 on the NF-κB signaling pathway in LPS-induced RAW264.7 cells. (A) Representative Western blot images of key proteins in the NF-κB pathway; (B) p-IKKα/β protein and; (C) IKKα/β mRNA expression levels; (D, E) Protein expression levels of p-IκB-α and IκB-α; (F) p-p65 protein and; (G) p-p65 mRNA expression levels. Data are presented as the mean ± SD from three independent experiments. #$P < 0.05$, ##$P < 0.01$ vs. control group; *$P < 0.05$, **$P < 0.01$ vs. LPS group.

Formula 1 promotes the activation of the Nrf2/HO-1 pathway

Oxidative stress induced by LPS contributes to inflammation by indirectly promoting cytokine expression in macrophages (Kang and Hyun, 2017). The Nrf2/HO-1 signaling axis acts as an essential cellular protective system, protecting against oxidative stress during inflammation (Li *et al.*, 2018). Moreover, Nrf2 is known to directly regulate the expression of pro-inflammatory genes, such as IL-1β and IL-6 (Kobayashi *et al.*, 2016). Based on network pharmacology predictions linking VEGFR2 and cytochrome P450 enzymes to Nrf2 activation (Du *et al.*, 2025), this pathway was explored. As depicted in figure 9, treatment with Formula 1 substantially enhanced the nuclear translocation of Nrf2 and upregulated the protein levels of its downstream target, HO-1, in both time- and concentration-dependent manners.

DISCUSSION

The development of multi-target strategies is important for addressing immune dysregulation (Kim *et al.*, 2020). Although terpenoids such as (-)-Linalool, (-)-Borneol and β-Caryophyllene have recognized immunomodulatory properties, the comprehensive immunopharmacology of specific multi-terpene combinations remains under-explored. The present study was designed to addresses this gap by showing that a fixed-ratio (5:23:26) combination of these three terpenoids (Formula 1) exerts an enhanced anti-inflammatory effect through coordinated regulation of AA metabolism, NF-κB and Nrf2/HO-1.

This effect was validated using two different but complementary pharmacological models. In the *ex-vivo* IgE-mediated allergic reaction model, a sensitized guinea pig ileum was used to measure SRS-A release as an indicator of type I hypersensitivity (Wang *et al.*, 2014). This model is capable of measuring the extent of ileal smooth muscle contraction induced by SRS-A released from sensitized tissues (Hu *et al.*, 2014), thereby enabling quantitative analysis of SRS-A release from sensitized tissues. Among all the combinations tested, Formula 1 achieved an inhibition rate of 79.87% ($P < 0.01$) against SRS-A release, which was higher than that of Formula 2 and Formula 3.

Article

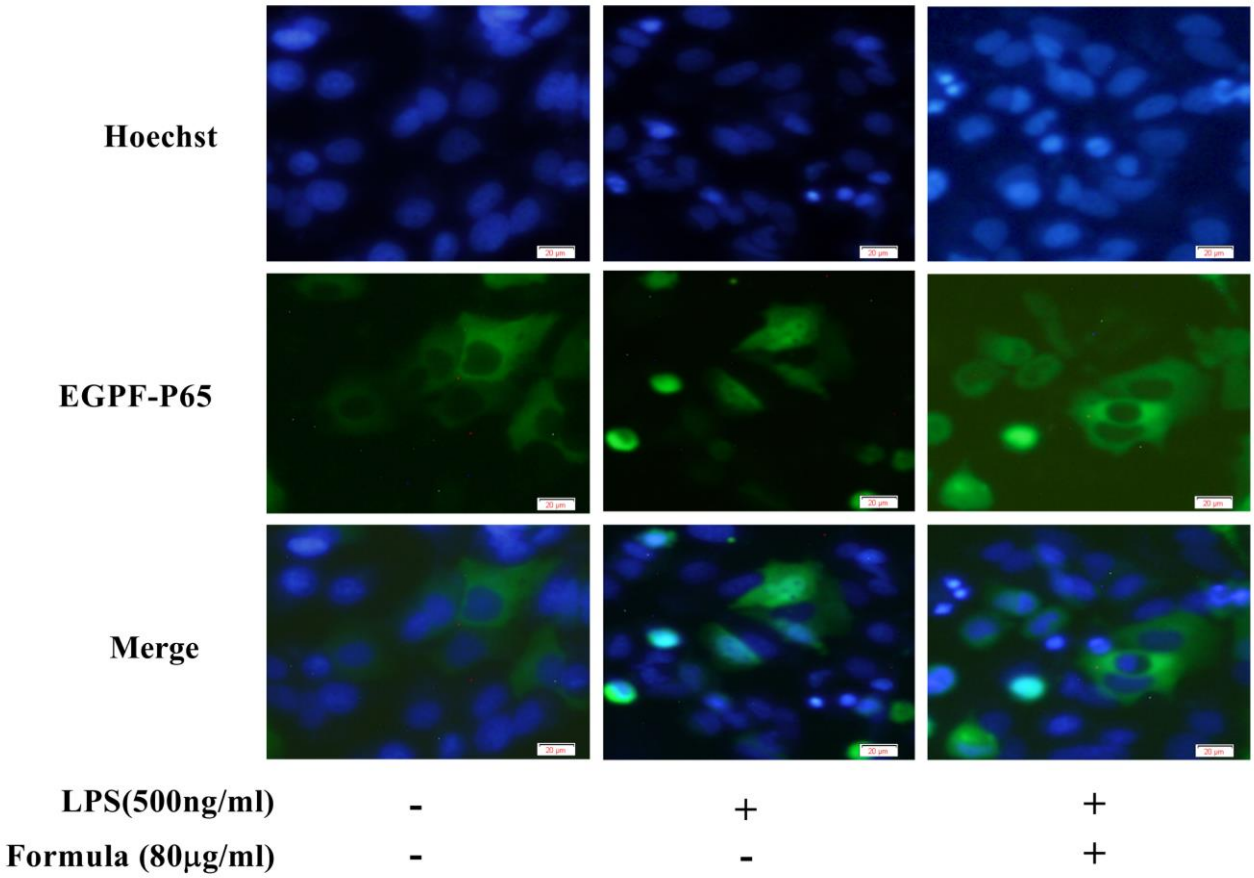


Fig. 8: Effect of Formula 1 on LPS-induced nuclear translocation of p65 in MCF-7 cells. Cells were transfected with pEGFP-N1-p65 and then treated with LPS (500 ng/mL) in the absence or presence of Formula 1 (80 μg/mL) for 12 h. The subcellular localization of EGFP-p65 was visualized by fluorescence microscopy. Scale bar = 20 μm (40×). Images are representative of three independent experiments ($n = 3$ per group). Nuclear translocation of p65 (green fluorescence) was assessed by the accumulation of EGFP-p65 in the nucleus.

Formula 1 also exceeded each component and the positive control quercetin (70.48%, $P < 0.01$). Similar results were obtained in the LPS-stimulated macrophage model. At 80 μg/mL, Formula 1 and (-)-Linalool markedly reduced the production of PGE2, LTB4, NO and iNOS ($P < 0.01$). (-)-Borneol only affected on iNOS ($P < 0.01$) and β-Caryophyllene only reduced PGE2 and LTB4 ($P < 0.01$). Notably, even when the dose of (-)-Linalool in Formula 1 was reduced to one-tenth of its original amount, the combination still showed efficacy comparable to the full-dose single compound. This indicates that there is an enhanced interaction among the three components which is not driven by a single dominant component.

Although the SRS-A guinea pig ileum model and LPS-stimulated RAW264.7 macrophage model reflect distinct inflammatory subtypes, they converge on the identical AA metabolic cascade and NF-κB signaling pathway. In the SRS-A allergic *ex-vivo* model, antigen challenge triggers leukotriene secretion (LTB4, LTC4, LTD4) via the 5-LOX pathway and subsequent smooth muscle contraction. In the LPS-induced innate inflammatory model, NF-κB activation further promotes COX-2 and 5-LOX expression, driving PGE2 and LTB4 generation (Rahmawati *et al.*, 2024). Accordingly, AA metabolism and NF-κB serve as conserved mechanistic hubs shared by both allergic and innate inflammation (Ren *et al.*, 2025).

These two complementary models were adopted to comprehensively verify the broad-spectrum anti-inflammatory effects of Formula 1 on common inflammatory cascades, including attenuated leukotriene-mediated smooth muscle contraction and decreased pro-inflammatory eicosanoids in macrophages. Collectively, the combination targets central innate inflammatory pathways rather than isolated allergic pathological processes (Kim *et al.*, 2026). For mechanistic insight, network pharmacology predicted AA metabolism, IL-17 and lipid/atherosclerosis as key pathways and identified 12 core targets including PTGS2/COX-2. Experimental validation confirmed only the AA metabolism pathway and PTGS2/COX-2 (1/3 pathways, 1/12 targets).

Article

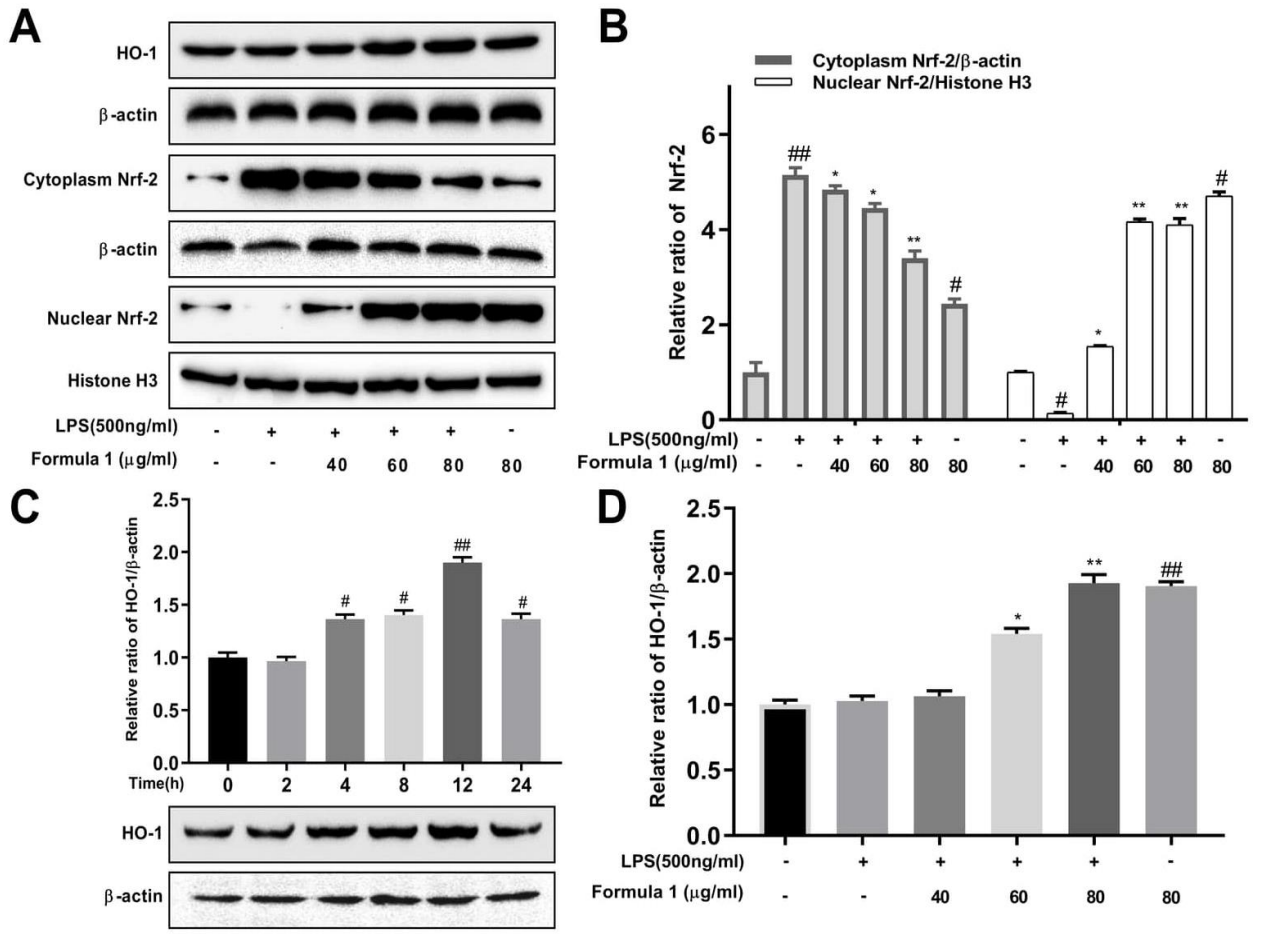


Fig. 9: Effects of Formula 1 on the Nrf2/HO-1 pathway in LPS-induced RAW264.7 cells. (A) Representative Western blot analysis of HO-1 expression in whole-cell lysates and Nrf2 distribution in nuclear and cytoplasmic fractions. β-actin and histone H3 were used as loading controls for cytoplasmic and nuclear proteins, respectively; (B) Quantitative analysis of Nrf2 protein levels in the nucleus and cytoplasm (normalized to loading controls); (C) Time-dependent expression of HO-1 protein following Formula 1 treatment (0-24 h); (D) Concentration-dependent effects of Formula 1 (0-80 μg/mL) on HO-1 protein expression. Data are presented as the mean ± SD from three independent experiments. #$P < 0.05$, ##$P < 0.01$ vs. control group; *$P < 0.05$, **$P < 0.01$ vs. LPS group.

Future studies should explore whether Formula 1 modulates IL-17 signaling, lipid metabolism and targets like RXRA, IL-6 and KDR, in chronic inflammation settings. Molecular docking results showed binding energies of -7.9 kcal/mol for β-Caryophyllene with PTGS2 and -9.9 kcal/mol for (-)-Linalool with KDR, suggesting that these interactions may mediate the anti-inflammatory effects of the combination. For the experimentally validated target PTGS2, a detailed analysis of the binding mode was performed. β-Caryophyllene binds within the cyclooxygenase active site, forming multiple hydrophobic interactions such as VAL349, LEU352, MET522 and hydrogen bonds such as with SER119, ARG120. Importantly, the binding residues of β-Caryophyllene are highly consistent with those of classical COX-2 inhibitors (Musa *et al.*, 2024). Three core residues (TYR385, VAL523 and ARG120) are fully shared and hydrophobic residues such as LEU352, LEU384, ALA527, TRP387, TYR348 and VAL349 are 100% coincident with those reported in the literature for standard COX-2 inhibitors (Elewa *et al.*, 2024). Overall, the binding residues of β-Caryophyllene overlap significantly with the key interaction sites of known COX-2 inhibitors, indicating a highly similar binding mode. These findings support the anti-inflammatory potential of β-Caryophyllene. For the other predicted targets (KDR, SLC6A3, CYP2C9, RXRA), docking results are presented in figure 5. However, because only PTGS2 was experimentally validated in this study, the detailed discussion has been focused on PTGS2. The remaining docking data are provided as computational predictions that may inform future research. A detailed list of interacting residues for the β-Caryophyllene with PTGS2 complex is provided in Supplementary figure S5.

Importantly, the data extend beyond predictions: while network pharmacology suggested involvement of downstream cytokines like IL-6, Formula 1 was found to

Article

acts at upstream nodes, regulating IKK complex phosphorylation and Nrf2 nuclear translocation, thereby achieving coordinated inhibition of multiple downstream pathways. Thus, computational predictions are incomplete without empirical testing.

The findings demonstrate that Formula 1 modulates inflammation through three distinct pathways. First, it attenuates the AA cascade by reducing COX-2, 5-LOX and FLAP, decreasing PGE2 and LTB4 (Yan *et al.*, 2024). Second, it suppresses NF-κB by inhibiting IKKα/β, IκBα and p65 nuclear translocation, reducing TNF-α and IL-1β. Third, it increases the Nrf2/HO-1 antioxidant axis, promoting Nrf2 nuclear accumulation and HO-1 expression, which also limits NF-κB activity. This integrated regulatory network offers advantages over single-point inhibition. In LPS-stimulated macrophages, Formula 1 reduced apoptosis (Hoechst 33342/PI staining), which likely reflects direct cytoprotection via Nrf2/HO-1 activation and indirect attenuation of pro-apoptotic inflammatory signals due to NF-κB suppression. Based on the literature, Nrf2 can also promote M2-like polarization and antagonistic crosstalk between Nrf2 and NF-κB may contribute to the coordinated anti-apoptotic effect (Wakai *et al.*, 2026). However, the precise contribution of apoptosis reduction to the overall anti-inflammatory outcome remains to be dissected and further studies are needed to establish causality.

Three unresolved challenges exist in terpenoid anti-inflammatory research: lack of experimental validation for multi-terpenoid combinations, missing pathway evidence for fixed-ratio mixtures and unverified natural ratios. As highlighted in recent reviews, the theoretical potential of terpenoid synergy has been discussed, yet direct experimental validation remains scarce (Begh *et al.*, 2025). Moreover, although network pharmacology has been increasingly applied to predict anti-inflammatory pathways (Liu and Liu, 2025) and metabolomic profiling has confirmed the presence of bioactive terpenoids in medicinal plants such as *Blumea balsamifera* (Maulydia *et al.*, 2025), the specific questions of whether a fixed natural ratio exerts superior effects and what pathways are involved have not been experimentally addressed. Our study directly fills these gaps. *In-vitro* and *ex-vivo* is provided for a fixed-ratio (5:23:26) combination of (-)-Linalool, (-)-Borneol and β-Caryophyllene. Using the HSA model and dose reduction experiments, a dominant component effect was ruled. Mechanistically, Formula 1 simultaneously reduces AA metabolism, inhibits NF-κB and increases Nrf2/HO-1, a tripartite regulation not previously shown for a defined ternary monoterpenoid combination. Thus, the present work supports multi-target anti-inflammatory strategies.

Formula 1 uses component proportions derived from an anti-inflammatory plant. This specific ratio was shown to work better than other ratios or single compounds. The natural compatibility ratio provides a reference for quality standardization, but further validation is needed (Rudrapal *et al.*, 2023). From a drug development perspective, the combination shows preliminary pharmacological potential, though the poor oral bioavailability and volatility of terpenoids remain challenges that future formulation strategies, such as cyclodextrin inclusion or nanoemulsions, could help address these issues (Li *et al.*, 2025). A limitation is that classical CI/Bliss analysis could not be applied due to the fixed-ratio design (each terpenoid at a much lower individual dose) and the single-concentration SRS-A assay (Ma *et al.*, 2025). Following the 3R principle, the HSA model was used as a conservative alternative. The HSA model demonstrated that Formula 1 achieved a 79.88% inhibition rate, compared to 57.81% for the most effective single component at the same total concentration, despite each terpenoid being present at only one-tenth to one-third of its single-agent dose. Although $n = 3$ is limited, the extremely low inter-replicate variability (SD = 0.353%) demonstrates good reproducibility. Other limitations include the lack of *in-vivo* pharmacodynamic data, the absence of validation on other immune cells such as T cells or dendritic cells (Georgakopoulou and Pitiriga, 2025) and the use of MCF-7 cells for NF-κB p65 nuclear translocation imaging due to technical difficulties with RAW264.7 macrophages. Although the NF-κB pathway is highly conserved, experimental data from RAW264.7 cells, including ELISA, qPCR and Western blotting, strongly indicate NF-κB inhibition, further studies are needed to clarify causality. These include direct visualization of p65 nuclear translocation in macrophages, as well as experiments using pathway inhibitors or gene-silencing techniques. In addition, future studies should evaluate the immunomodulatory effects of Formula 1 on these cells, especially in the context of adaptive immunity or allergic responses. The *in-vitro* and *ex-vivo* data thus support future *in-vivo* studies using animal models of acute or chronic inflammation.

CONCLUSION

Taken together, the present study shows that a defined combination of (-)-Linalool, (-)-Borneol and β-Caryophyllene exerts enhanced anti-inflammatory effect through coordinated modulation of multiple pathways. By suppressing the AA and NF-κB pathways while up-regulating the Nrf2/HO-1 axis, this combination achieved greater efficacy than its individual components. This finding provides a scientific basis for using traditional natural products in modern medicine and offers a candidate molecular combination for developing multi-target therapies against immune-mediated inflammatory diseases. Because of its favorable safety profile and well-defined mechanism, this combination warrants further preclinical and clinical testing. Such studies could help

Article in Press

address unmet clinical needs in chronic inflammatory diseases.

Acknowledgments
The authors would like to thank all members of the Engineering and Research Center for Southwest Bio-Pharmaceutical Resources of the National Education Ministry of China's labs for their technical assistance and support in various aspects of this work. Part of the experimental work, as well as all data compilation and manuscript writing, was completed during the authors' employment at Sansui People's Hospital. We sincerely thank the hospital for its sustained institutional support and academic encouragement. The use of DeepSeek for English language polishing and grammar checking during the preparation of this manuscript is acknowledged. All core research concepts, experimental design, data collection, analysis and interpretation were independently completed by the authors, who take full responsibility for the accuracy and integrity of all the content presented in this manuscript.

Authors' contributions
Wan Lin Wang: Methodology, data curation, validation, visualization and writing the original draft; Kazi Sabnam Siddiqua: Manuscript writing and correction; Yue Gao and Jiarong Yin: Formal analysis; Qiong Yi: Supervision; Lu Wang: Conceptualization, resources and revision of manuscript. All authors read and approved the published version.

Funding
This research was supported by the National Research Foundation of the National Natural Science Foundation of China (No.32160849, 3227305 and 31760747).

Data availability statement
The datasets generated and/or analysed during the current study are available from the corresponding author on reasonable request.

Ethical approval
The animal experiments were conducted in accordance with the 'Guiding Principles in the Care and Use of Animals' (China) and approved by the Animal Experimental Ethics Committee of Guizhou University (Document No. EAE–GZU–2021–E026). This study was performed in adherence with the ARRIVE guidelines. See supplementary file for the ARRIVE checklist.

Conflict of interest
The authors declare no competing interests.

REFERENCES

Begh MZA, Khan J, Al Amin M, Sweilam SH, Dharmamoorthy G, Gupta JK, Sangeetha J, Lokeshvar R, Nafady MH and Ahmad I (2025). Monoterpenoid synergy: A new frontier in biological applications. *Naunyn Schmiedebergs Arch Pharmacol*., **398**(1): 103-124.

Capece D, Verzella D, Flati I, Arboretto P, Cornice J and Franzoso G (2022). NF-κB: Blending metabolism, immunity and inflammation. *Trends Immunol.*, **43**(9): 757-775.

Chen S, Yu Y, Su Y, Lian X, Jiang L, Li Z, Zhang M, Gao Y, Zhang H, Zhu X, Ke J and Chen X (2025). Screening and identification of host signaling pathways for alleviating influenza-induced production of pro-inflammatory cytokines, IP-10, IL-8 and MCP-1, using a U937 cell-based influenza model. *Front. Microbiol.*, **16**: 1535002.

Choi J, Jeon HJ, Park J, Sonn SK, Lee M, Lee M, You HJ, Kim G, Kim J and Lee MH (2010). Anti-atherogenic effect of BHB-TZD having inhibitory activities on cyclooxygenase and 5-lipoxygenase in hyperlipidemic mice. *Atherosclerosis*., **212**(1): 146-152.

Cong Y, Bearss J, Mani V, Lackemeyer M, Pahar B, Huzella LM, Kollins E, Mazur S, Dixit S and Lembirik S (2025). Large-particle aerosol exposure to the Bangladesh or Malaysia strain of Nipah virus results in markedly divergent disease presentation in African Green Monkeys. *PLoS Pathog.*, **21**(12): e1013835.

Cortez I, Gaffney CM, Vichare R, Crelli CV, Liu L, Lee E, Edralin J, Nichols JM, Pham HV and Mehdi S (2024). Neuromuscular polytrauma pain is resolved by macrophage COX-2 nanoimmunomodulation. *Int. J. Nanomed.***19**: 7253-7271.

Cui S, Chen C, Xiong W, Yang C and Wang W (2026). Investigating the mechanism of swertia davidii franch. in treating acute liver injury by integrating network pharmacology. *Chem. Biodivers.*, **23**(2): e2932.

D Orazio S and Mattoscio D (2024). Dysregulation of the arachidonic acid pathway in cystic fibrosis: Implications for chronic inflammation and disease progression. *Pharmaceuticals (Basel).*, **17**(9): 1185.

Du Q, Liu K, Li Y, Wang X, Liu X, Zhao J and Wang X (2025). Inhibition of CYP450 family 1 subfamily B member 1 (CYP1B1) expression in macrophage reduces the inflammatory response in type 2 diabetes mellitus combined with tuberculosis. *Front Endocrinol (Lausanne).*, **16**: 1617292.

Elewa M, Shehda M, Hanna PA, Said MM, Ramadan S, Barakat A and Aziz YMA (2024). Development of a selective COX-2 inhibitor: From synthesis to enhanced efficacy via nano-formulation. *RSC Adv.*, **14**(45): 32721-32732.

Georgakopoulou VE and Pitiriga VC (2025). Immunomodulation in respiratory syncytial virus infection: mechanisms, therapeutic targets and clinical implications. *Microorganisms*., **13**(8): 1876.

Hu Y, Liu Z, Yu X, Pasricha PJ, Undem BJ and Yu S (2014). Increased acid responsiveness in vagal sensory

Article in Press

neurons in a guinea pig model of eosinophilic esophagitis. *Am. J. Physiol.-Gastroint. Liver Physiol.*, **307**(2): G149-G157.

Hu YF, Tang JY, Sun HY, Li YP, Yu FL, Zhang GC, Chen JL, Xu H, Zhong ZQ, Huang C, Hu KF, Xie M and Yang JH (2025). Artesunate modulates the tumor microenvironment via STAT1/ IRF1-mediated TAM repolarization and T cell activation in non-small cell lung cancer. *Phytomedicine*., **146**: 157085

Huang L, Wang J, Fang B, Meric-Bernstam F, Roth JA and Ha MJ (2022). CombPDX: A unified statistical framework for evaluating drug synergism in patient-derived xenografts. *Sci. Rep.*, **12**(1): 12984.

Jiang M, Sun C, Wang B, Huang Q, Hu Q and Che X (2026). Analysis of the molecular mechanism underlying di (2-ethylhexyl) phthalate-induced bladder carcinogenesis via network toxicology and molecular docking approaches: An observational study. *Medicine. (Baltimore).*, **105**(6): e47378.

Kang KA and Hyun JW (2017). Oxidative stress, Nrf2 and epigenetic modification contribute to anticancer drug resistance. *Toxicol. Res.*, **33**(1): 1-5.

Karaoli A, Mintis DG, Tzoupis H, Kiranoudis CT, Lynch I, Melagraki G and Afantitis A (2026). Molecular dynamics simulations of temperature-dependent PET binding in PETase, ThermoPETase and FAST-PETase. *RSC Adv.*, **16**(18): 16050.

Kim J, Heo S, Kim E, Kang N and Heo S (2026). 2-Bromo-5-hydroxy-4-methoxybenzaldehyde exhibits anti-inflammatory effects through the inactivation of ERK, JNK and NF-kB pathways in RAW 264.7 cells. *Phycology*., **6**(1): 10.

Kim T, Song B, Cho KS and Lee I (2020). Therapeutic potential of volatile terpenes and terpenoids from forests for inflammatory diseases. *Int. J. Mol. Sci.*, **21**(6): 2187.

Kobayashi EH, Suzuki T, Funayama R, Nagashima T, Hayashi M, Sekine H, Tanaka N, Moriguchi T, Motohashi H and Nakayama K (2016). Nrf2 suppresses macrophage inflammatory response by blocking proinflammatory cytokine transcription. *Nat. Commun.*, **7**(1): 11624.

Kumar A, Dubey AK and Misra G (2025). Role of cytokines in chikungunya infections. Cytokine response against major human viral infections, 1st ed., Academic Press, London, pp. 165-181.

Li J, Liang H, Liu L, Gao X, Liu Y, Zhang M, Yuan X, Ren S and Zhang W (2025). Structural diversity and biological activities of terpenoids derived from Tripterygium wilfordii Hook. f. *RSC Adv.*, **15**(16): 12594-12608.

Li S, Dai Q, Zhang S, Liu Y, Yu Q, Tan F, Lu S, Wang Q, Chen J and Huang H (2018). Ulinastatin attenuates LPS-induced inflammation in mouse macrophage RAW264. 7 cells by inhibiting the JNK/NF-κB signaling pathway and activating the PI3K/Akt/Nrf2 pathway. *Acta Pharmacol. Sin.*, **39**(8): 1294-1304.

Liao J, Xie X, Wang W, Gao Y, Cai Y, Peng J, Li T, Yi Q, He C and Wang L (2021). Anti-inflammatory activity of essential oil from leaves of Blumea balsamifera (L.) DC through inhibiting TLR4/NF-kB signaling pathways and NLRP3 inflammasome activation in LPS-induced RAW264. 7 macrophage cells. *J. Essent. Oil-Bear. Plants*., **24**(2): 160-176.

Liu S, Chen P, Li Y, Pan Z, Zhang C, Li A, Huang C, Zheng H, Chen L and Shen C (2026). Bupleurum Chinese ameliorates metabolic-associated fatty liver disease by modulating sirtuin 6. *Phytomedicine*., 157905.

Liu Z and Liu J (2025). Integrative network pharmacology and experimental validation of anti-inflammatory triterpenoids from hawthorn leaves. *Sci. Rep.*, **15**(1): 21765.

Luo Y, Xue E, Zhao Y, Lu H, Xiang D, Zhou Y, Zhan J, Li Z and Sun F (2025). Integrative network and computational toxicology reveal the molecular mechanisms in PFOA-induced spermatogenic disorder. *J. Environ. Manage.*, **386**: 125754.

Ma P, Liu W, Wen H, Shen M, Luo Y and Xie J (2025). Comparative study of rosemary extract, TBHQ, citric acid and their composite antioxidants on the overall quality of peanuts and evaluation of their synergistic antioxidant properties and interaction. *Food Res. Int.*, **214**: 116623.

Maulydia NB, Khairan K, Tallei TE and Idroes R (2025). Metabolomic profiling and anti-inflammatory activity of Blumea balsamifera: Insights from in silico and *in-vitro* studies. *Pharmacia*., **72**: 1-15.

Musa MS, Miah MS, Munni YA, Patwary MAM, Kazi M and Matin MM (2024). Synthesis and elucidation of strained galactopyronose esters as selective cyclooxygenase-2 inhibitor: A comprehensive computational approach. *RSC Adv.*, **14**(41): 30469-30481.

Niu Z, Li X, Yang X and Sun Z (2024). Protective effects of sinomenine against dextran sulfate sodium-induced ulcerative colitis in rats via alteration of HO-1/Nrf2 and inflammatory pathway. *Inflammopharmacology*., **32**(3): 2007-2022.

Pan M, Wang P, Wang X, Wang Z, Zhang Z, Yang K, Liu W, Ma W and Liu X (2026). Insights into the potential mechanism of Beiqishen Jiangtang Granule in the treatment of type 2 diabetes nephropathy: A study based on network pharmacology, molecular docking and biological validation. *Medicine. (Baltimore).*, **105**(7): e47533.

Pan Y, Liu X, Wang S, Chen L, Li A, Chi Q, Ku X, Xu K and Wang C (2026). Coniferyl aldehyde in ginger-eucommiae cortex enhances osteoarthritis treatment by modulating ALDOA and H3K23la histone lactylation. *Phytomedicine*., **152**: 157852.

Qidwai T (2024). Cytokine storm in COVID-19 and malaria: Annals of pro-inflammatory cytokines. *Cytokine*., **173**: 156420.

Article in Press

Rahmawati SI, Indriani DW, Ningsih FN, Hardhiyuna M, Firdayani F, Ahmadi P, Rosyidah AL, Septiana E, Dharmayanti NLPI and Bayu A (2024). Dual anti-inflammatory activities of COX-2/5-LOX driven by kratom alkaloid extracts in lipopolysaccharide-induced RAW 264.7 cells. *Sci. Rep.*, **14**(1): 28993.

Ren S, Lu L, Su H, Li Z, Li S, Pan J, Liu Y, Ji G and Xu H (2025). Regulating arachidonic acid metabolism: A novel strategy to prevent colorectal inflammatory cancer transformation. *J. Cancer*., **16**(14): 4155.

Riaz R, Younis W, Uttra AM, Malik MNH, Manzoor W, Qasim S, Hasan UH and Mushtaq (2025). Anti-arthritic and anti-inflammatory activity of linalool against formaldehyde and complete Freund's adjuvant induced arthritis in rats. *Biochem. Biophys. Res. Commun.*, **752**: 151462.

Rudrapal M, Eltayeb WA, Rakshit G, El-Arabey AA, Khan J, Aldosari SM, Alshehri B and Abdalla M (2023). Dual synergistic inhibition of COX and LOX by potential chemicals from Indian daily spices investigated through detailed computational studies. *Sci. Rep.*, **13**(1): 8656.

Taniguchi K and Karin M (2018). NF-κB, inflammation, immunity and cancer: Coming of age. *Nat. Rev. Immunol.*, **18**(5): 309-324.

Vlot AH, Aniceto N, Menden MP, Ulrich-Merzenich G and Bender A (2019). Applying synergy metrics to combination screening data: Agreements, disagreements and pitfalls. *Drug Discov. Today*., **24**(12): 2286-2298.

Wakai T, Chinedu S and Afolabi I (2026). Heme oxygenase-1 and malaria pathogenesis. *Front. Immunol.*, **17**: 1777520.

Wang G, Wang X, Liu S, Qu M, Xia Y, Needleman BJ, Mikami DJ and Wood JD (2014). Innervation of enteric mast cells by primary spinal afferents in guinea pig and human small intestine. *Am. J. Physiol.-Gastroint. Liver Physiol.*, **307**(7): G719-G731.

Wang XS, Xie NL, Zhang HY, Zhou WH and Lei JD (2025). Isoorientin ameliorates macrophage pyroptosis and atherogenesis by reducing KDM4A levels and promoting SKP1-Cullin1-F-box E3 ligase-mediated NLRP3 ubiquitination. *Inflammation*., **48**(5): 3629-3648.

Wang Y, Yang Y, Meng T, Liu S, Liu J, Liu D, Laxman B, Chen S and Dong Z (2025). β-caryophyllene reduces inflammation to protect against ischemic stroke by suppressing HMGB1 signaling. *Mol. Med*., **31**(1): 112-114.

Wang Z, Jiang YP, Ge CY, Wang YX, He J, Chen J and Hou XJ (2024). Anti-inflammatory activity evaluation and molecular docking analysis of four new compounds isolated from M. oleifera seeds. *J. Mol. Struct.*, **1318**: 139269.

Wilkens M, Holtermann L, Stahl A, Stegmeyer RI, Nottebaum AF and Vestweber D (2024). Ubiquitination of VE-cadherin regulates inflammation-induced vascular permeability *in-vivo*. *EMBO Rep.*, **25**(9): 4013-4032.

Xianfang H, Wanlin W, Hongying W, Ruixiu L, Qiong Y and Lu W (2024). Blumea balsamifera (L.) DC oil alleviates LPS-induced inflammatory response in macrophages by affecting arachidonic acid metabolism via NF-κB nonclassical pathway. *J. Sun Yat-sen Univ. (Med. Sci.)*., **45**(2): 216-225.

Xiao S, Yu H, Guo Y, Cheng Y and Yao W (2025). The antibacterial and anti-inflammatory potential of *Cinnamomum camphora* chvar. borneol essential oil *in-vitro*. *Plants*., **14**(12): 1880.

Xu R, Zhang L, Pan H and Zhang Y (2024). Retinoid X receptor heterodimers in hepatic function: Structural insights and therapeutic potential. *Front. Pharmacol.*, **15**: 1464655.

Xueyan X, Tianzhen L, Wanlin W, Yue G, Qiong Y, Lu W and Yan X (2019). Analysis of chemical constituents and anti-inflammatory activity of *Blumea balsamifera* oil from different sources. *Tradit. Chin. Drug Res. Clin. Pharmacol*., **30**(09): 1069-1076.

Yaling C, Jiamei L, Junchao P, Yue G, Wanlin W, Qiong Y and Lu W (2021). Screening of anti-inflammatory substances from *Blumea balsamifera*(L.)DC.oil and their effects on inflammatory factors. *Nat. Prod. Res. Dev*., **33**(3): 402-409.

Yan Y, Di F, Zhang R, Song L, Zhang R and Qiu J (2024). Arachidonic acid inhibit granulosa cell function by affecting metabolic function of liver in brown adipose transplantation rats. *J. Ovarian Res.*, **17**(1): 14-43.

Zeng Q, Xiao W, Zhang H, Liu W, Wang X, Li Z, Han Y, Wang Z, Li S, Yang J and Ouyang W (2025). α-spinasterol isolated from Achyranthes aspera L. ameliorates inflammation via NF-κB and Nrf2/HO-1 pathways. *Sci. Rep.*, **15**(1): 5710-5723.

Zhang MZ, Wang YF, Li QY, Luo YF, Tao L, Lai DL, Zhang Y, Chu L, Shen QW, Liu DB and Wu YY (2024). Ultrasound-assisted extraction of polysaccharides from *Ginkgo biloba*: Process optimization, composition and anti-inflammatory activity. *Heliyon*., **10**(18): e37811.

Article in Press